DOI: 10.1002/ente.201402174

Roll-to-Roll Sputter Coating of Aluminum Cathodes for Large-Scale Fabrication of Organic Photovoltaic Devices

Matthew J. Griffith,*[a] Nathan A. Cooling,[a] Ben Vaughan,[a] Kane M. O'Donnell,[b] Mohammed F. Al-Mudhaffer,[a] Alaa Al-Ahmad,[a] Mahir Noori,[a] Furqan Almyahi,[a] Warwick J. Belcher,[a] and Paul C. Dastoor[a]

We report the demonstration of sputter-coated aluminum contacts directly onto P3HT:PCBM organic photovoltaic devices using a R2R process without detrimentally influencing the performance of the devices. The final sputtered devices do not require any protective buffer layers to produce efficient performance. Depth profiling analysis of sputtered films using X-ray photoelectron spectroscopy (XPS) indicated the presence of a 5–6 nm insulating oxide layer generated at the cathode interface for all sputtering target power densities greater than 1.4 $W cm^{-2}$. The aluminum penetration into the P3HT:PCBM film was found to be consistent with the depth of this oxide layer, suggesting that aluminum penetration into the organic film is not the primary reason for performance limitations in sputtered devices. Introduction of thermally evaporated aluminum buffer layers prior to deposition of sputtered aluminum cathodes demonstrated that the performance of devices after annealing matched those of reference devices prepared with no sputtering for a buffer layer thickness of only 20 nm. Further analysis of the device J--V curves revealed an S-shaped kink prior to annealing, indicating that the major reason for the poor performance in sputtered devices was the introduction of a charge extraction barrier at the cathode, which was subsequently removed upon annealing. Rigorous removal of oxygen from the sputtering chamber prior to aluminum deposition onto the P3HT:PCBM active layer was subsequently observed to produce a device with an efficiency close to that of the thermally evaporated reference device without the requirement for evaporated buffer layers. The results presented here highlight a pathway towards an alternative R2R cathode fabrication technique that allows the highly efficient aluminum cathodes employed in small-scale devices to be transferred onto large-scale, flexible, and low-cost R2R printed organic electronic devices.

Introduction

Solution-processed bulk-heterojunction organic photovoltaic (OPV) devices have received significant research interest over the past two decades due to their enormous potential for low-cost power production.[1] The key advantage of OPVs is that the polymer blend materials can be formed into inks that can be printed at high speeds across large areas using roll-to-roll (R2R) processing techniques.[2] However, despite potential module production costs reaching values as low as \$8 (Australian) per square meter,[3] transferring this technology from the laboratory scale, where small-scale devices with power conversion efficiencies of up to 12% have been demonstrated,[4] into the large-scale production arena presents some unique challenges. Generating uniform thin layers while tailoring the fine structure, morphology, and charge extraction properties of the OPV layers across large areas is fraught with difficulty due to the challenge of controlling phase segregation and interlayer wettability using conventional printing procedures.[5] In particular, there is a distinct lack of printable electrode materials, with silver inks currently employed to create the cathode in the bulk of reported printed OPV structures. Though this approach has produced single modules with efficiencies exceeding 3% and has allowed upscaled manufacture to installations producing more than 10 kV by linking upwards of 100000 cells with efficiencies of 1.5% in series,[6] moving from thermally evaporated cathode deposition on the small scale to printed cathode deposition on the R2R scale remains a significant challenge.[7]

Sputtering of metal contacts has proven to be a successful route for mass production of liquid-crystal displays,[8] and presents some unique advantages compared to printable cathodes. The technology is compatible with large-area substrates, can deposit a range of materials including pure metals, alloys, and oxide semiconductors,[9,10] and does not suffer wettability issues, resulting in compatibility with a wide range of device architectures. Furthermore, sputtering

[a] Dr. M. J. Griffith, Dr. N. A. Cooling, Dr. B. Vaughan, M. F. Al-Mudhaffer, A. Al-Ahmad, M. Noori, F. Almyahi, Dr. W. J. Belcher, Prof. P. C. Dastoor
Priority Research Centre for Organic Electronics
University of Newcastle
University Drive, Callaghan, NSW, 2308 (Australia)
E-mail: matthew.griffith@newcastle.edu.au

[b] Dr. K. M. O'Donnell
Department of Imaging and Applied Physics
Curtin University
Kent Street, Perth, WA, 6102 (Australia)

Part of a Special Issue on "Printed Energy Technologies". To view the complete issue, visit:
http://onlinelibrary.wiley.com/doi/10.1002/ente.v3.4/issuetoc

 © 2015 Wiley-VCH Verlag GmbH & Co. KGaA, Weinheim

the back contact would allow OPVs to be fabricated with aluminum cathodes, a material which is currently employed in the vast majority of high-efficiency small-scale devices, but which cannot be printed from solution due to its high reactivity in air.[11] Such efforts would allow R2R devices with asymmetric work functions to generate a photovoltage, negating the need to introduce specialized charge-selective transport layers, which can be difficult to print. However, previous attempts to create sputtered contacts in organic electronic devices, including OLEDs and OPVs, have observed significant performance limitations when depositing directly onto soft organic films.[12,13] Although the mechanism responsible for performance limitations remains unclear, the bombardment of the organic film with a flux of energetic gas ions and metal particles during sputtering has been postulated to deform devices through direct damage of the photoactive layer[14–17] or through penetration of the metal atoms through the soft organic layer to create a low shunt resistance.[18,19] Attempts to remedy damages caused by sputtering metal contacts onto organic films have shown some success. The deposition of buffer layers on top of the organic films, typically containing lithium ions,[8,20] and the application of intricate post-deposition thermal annealing treatments[21–24] have both been demonstrated as successful pathways to recover the performance of poorly functioning OLED and OPV devices prepared using sputtered contacts. However, a definitive mechanism for these procedures, and the underlying origin of poor performance in devices prepared with sputtered contacts, remains unclear.

There have been some attempts to introduce R2R-sputtered contacts into the fabrication of large-area printed OPV devices, however, these have focused on creating the initial contact and printing subsequent layers over the sputtered contact.[25,26] A key motivation for this work is to discover the mechanism that generates poor performance in OPV devices; the aluminum cathodes were sputtered directly onto the photoactive layer as a first step towards deployment of sputtering to create high efficiency devices on the R2R scale. In this article, we report that depositing aluminum directly onto P3HT:PCBM active layers using R2R sputtering equipment introduces an aluminum oxide charge-extraction barrier at the P3HT:PCBM interface, and the penetration of the energetic ions and atoms from sputtering does not hinder the performance of OPV devices to a significant extent. We then demonstrate that introducing extensive efforts to remove oxygen prior to sputtering deposition can create OPV devices with performance values close to those observed in reference devices prepared with thermally evaporated contacts. As such, the work presented here is the first practical demonstration of R2R-sputtered cathodes directly onto photoactive layers without introducing the need for any additional post-treatments to generate high performance. This result has significant implications for the large-scale manufacture of low-cost organic solar cells.

Results and Discussion

A suite of different printing and coating techniques have been gathering increasing research interest recently as potential routes towards the complete R2R processing of organic electronic devices on flexible substrates such as polyethylene terephthalate (PET). In accord with these research efforts, we have acquired several pieces of new equipment that allow for full R2R fabrication and lamination of printable OPV devices. The first of these is a Solar-1 coating line from Grafisk Maskinfabrik (Figure 1 a), which possesses a fully automated

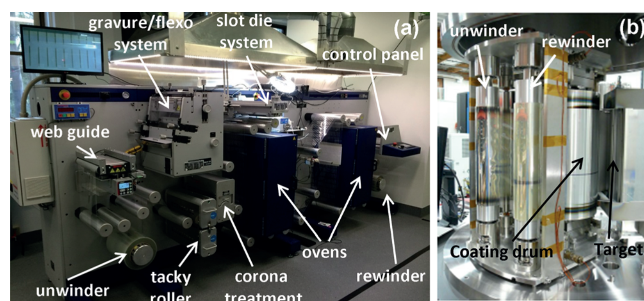

Figure 1. Photographs outlining the major components of the a) R2R solar coating line, and b) an internal view of the R2R sputter coater chamber installed at the Centre for Organic Electronics.

web alignment feedback element, a gravure and flexographic printing station, a separate slot–die coating unit, and two in-line heating ovens. This allows for the deposition and in-line thermal treatment of multiple patterned organic layers from different ink solutions in a single printing cycle. Such an approach has been shown to produce OPV devices printed at high speed with an efficiency exceeding 1.5 %.[5,6]

The aluminum cathode layers are fabricated by using a customized R2R DC magnetron sputter coater purchased from Semicore Equipment (Figure 1 b). This machine passes the flexible substrate around a cylindrical drum where it is exposed to three consecutive deposition zones from individually controlled targets. This allows for the ability to deposit multiple materials in a single run, enabling, for instance, single pass fabrication of emerging materials in the R2R fabrication space such as indium-tin oxide (ITO)–metal–ITO (IMI)[27] conductive plastic anodes or chromium–aluminum–chromium[9] cathode film structures. The choice of magnetron sputtering for cathode deposition in standard device architectures is divergent from the majority of previous efforts in the large-scale fabrication domain. Here we utilize the R2R sputter coater to examine the feasibility of depositing aluminum cathodes directly onto organic layers using an industrial-scale process.

The energy of the sputtering gas ions and the density of the gas environment are key features in the film quality and thickness deposited during the sputtering process. Ideally the sputtering conditions will be mild to minimize the potential for subsequent damage to the organic layers; however, this consideration must be balanced against the ability to produce

 © 2015 Wiley-VCH Verlag GmbH & Co. KGaA, Weinheim

a cathode of sufficient thickness during high-speed R2R fabrication. To calibrate the R2R coating system and discover the optimum coating conditions, the PET web was sputtered at a range of different target powers and chamber pressures. The resulting film thicknesses were analysed using the optical density of the films, and the film quality was examined using an optical microscope with a 40× objective. Thickness values could only be determined accurately to an approximate limit of 70 nm due to restrictions with the highly absorbing sputtered films. The measured aluminum film thickness exhibited a linear dependence on the target power in the range that could be accurately determined (Figure 2a). Knowing the dimensions of the target yields a defined deposition zone, and the speed of the web during coating can be used to compute the active sputtering time and thus convert the thickness to a sputtering rate. From the data in Figure 2a, a sputtering rate of 1 $nm\,s^{-1}$ was determined at a target power of 500 W (power density = 1.4 $W\,cm^{-2}$), with this rate observed to vary linearly up to at least 2 kW (5.6 $W\,cm^{-2}$). It is expected that the sputtering rate would continue to increase linearly with target power, although the film thickness could not be reliably determined in this study. The aluminum thickness also exhibited a linear dependence on the argon pressure during sputtering (Figure 2b). The film thickness dropped by 18% between 2 and 20 mTorr (1 mTorr ≈ 1.3×10^{-6} bar), consistent with the decreased mean free path of the carrier gas in the sputtering chamber at increased pressure. Figure 2b indicates a drop in the sputtering rate of approximately 1% for every 1 mTorr increase in pressure with respect to the base value obtained at 2 mTorr. The uniformity of the film thickness across the 300 mm PET web was examined using a sample transport feature coupled to a UV-visible spectrometer. The thickness of the aluminum layer was determined in 25 mm steps across the web after sputtering at various target powers, with the zero position adjacent with the outer edge of the web and the center of the web located at a sample translation of 150 mm (Figure 2c). The lower target powers do not coat the aluminum film uniformly out to the edges of the web, with powers of 1 kW and below exhibiting thickness values below 80% of the maximum at the outer 15% of each edge. Given this result, it was decided that a target power of 1.5 kW was the minimum required to generate relatively uniform thickness across the majority of the PET substrate. This value still leaves the outer 1–2 cm coated at a much lower aluminum thickness; however this space would be used for sealant and encapsulation in a fabricated module and is therefore considered acceptable. As the R2R process requires deposition rates to be maximized, it was decided that a low sputtering process pressure of 2 mTorr was the ideal condition to match with the applied target power of 1.5 kW. These conditions strike an ideal compromise between uniform substrate coverage, reduced power for minimizing energetic particle damage to the organic films, and fast deposition rates.

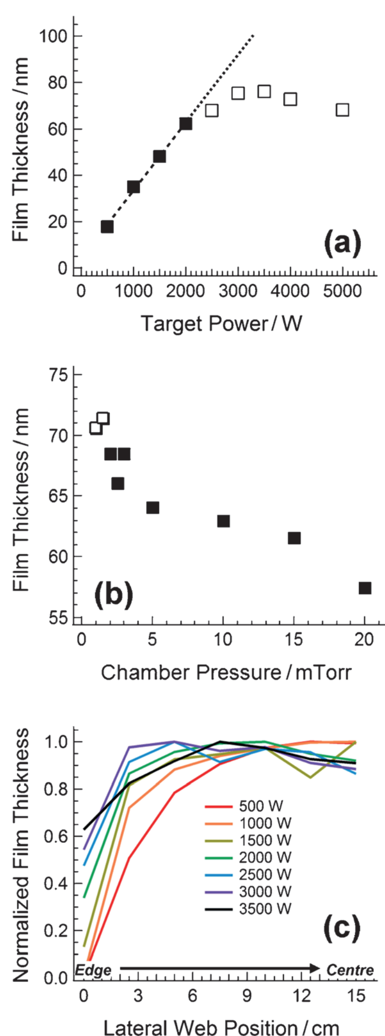

Figure 2. The aluminum film thickness determined by transmission measurements for films prepared using the roll-to-roll sputter coater with a) different target powers at a constant pressure of 2 mTorr (1 mTorr ≈ 1.3×10^{-6} bar), and b) different sputtering pressures at a constant target power of 2 kW. Film thicknesses above 70 nm are shown as open symbols to indicate they are above the limit that can be accurately determined from transmission measurements. c) The lateral thickness profile was measured from the edge of the PET web (0 cm) towards the center (15 cm) for films prepared using different target powers.

To probe the mechanism responsible for the documented poor performance of metal contacts sputtered directly onto organic layers, model small-scale films were prepared on glass substrates. 100 nm films prepared from a 1:1 blended solution of poly(3-hexylthiophene) (P3HT) and phenyl-C_{61}-butyric acid methyl ester (PCBM) were sputtered with a 100 nm aluminum contact using various target powers. X-ray photoelectron spectroscopy (XPS) depth profiling measurements were then performed on these films using an argon cluster ion etching source. This technique provides excellent depth resolution with negligible ion beam induced intermixing of the analyzed layers due to an essentially damage-free sputtering process.[28] Spectral analysis of the XPS signal revealed the presence of a strong Al2p peak from the sputtered contact, C1s and S2p peaks from the blended polymer-acceptor layer, and the presence of a peak in the O1s signal in the interfacial region between the organic film and aluminum contact (Figure 3a). The O1s and Al2p signals in this

 © 2015 Wiley-VCH Verlag GmbH & Co. KGaA, Weinheim

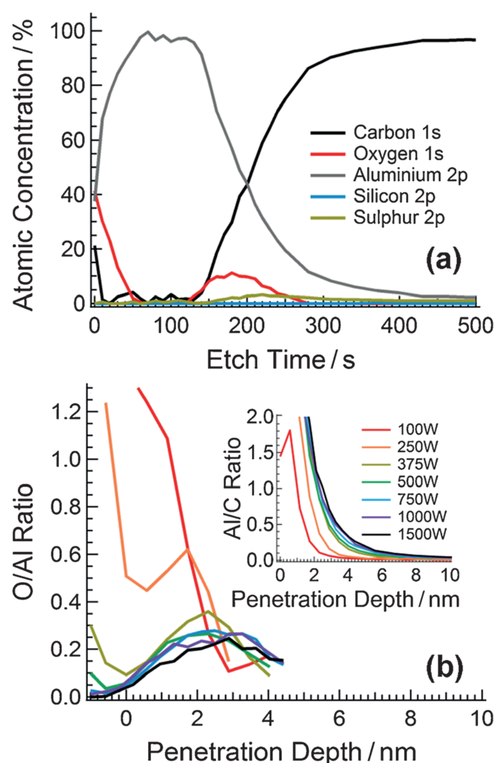

Figure 3. a) An XPS depth profile of a P3HT:PCBM film covered with 100 nm of aluminum by sputtering with a target power of 1500 W, showing carbon (black), oxygen (red), aluminum (gray), silicon (blue), and sulphur (yellow). b) The O/Al ratio determined as a function of depth for P3HT:PCBM films covered with 100 nm of aluminum by sputtering at various target powers. The inset shows the Al/C ratio with respect to penetration depth into the P3HT:PCBM film.

region are consistent with the presence of an interfacial aluminum oxide species, rather than any trapped water or other oxygen containing contaminants. The presence of a highly insulating oxide layer at the interface will likely be detrimental to electron injection from the fullerene acceptor into the metal contact, and this may be one reason for the poor performance typically observed in devices prepared with sputtered cathodes. Another often-cited mechanism for this poor performance is the possibility of penetration of sputtered material into the organic layer, and subsequent damage to the film structure. The depth profile shown in Figure 3a confirms that the aluminum does penetrate into the polymer film. XPS depth profiling measurements typically show some interlayer mixing caused by the resolution of the ion beam and surface roughness of the interface, however in this case, the aluminum signal extends a significant period beyond the interface, allowing the signal to be distinguished from this interlayer resolution limit. Thus the XPS data also confirms a penetration of sputtered atoms into the organic layer, which may result in damage to the film.

To further probe the two potential limiting mechanisms, the O/Al ratio and the Al/C ratio were both plotted against penetration depth into the organic film (Figure 3b). The former ratio provides information on the formation of an insulating oxide layer, whereas the latter ratio can be used to probe the penetration of the conducting aluminum atoms into the photoactive film. As the organic films for all samples were prepared using identical fabrication conditions, etching completely through the P3HT:PCBM layer in a test sample (as identified by a sharp rise in the Si 2p peak from the underlying glass substrate) provides a method to convert the etch time into film penetration depth, given the known 100 nm thickness of the films. Figure 3b shows that the O/Al ratios for the oxide layers formed from sputtering at low power levels are larger than those at higher powers, and this indicates a greater extent of oxidation in these samples. Moreover, at the very lowest powers (up to 250 W) the sputtered aluminum film is essentially fully oxidized throughout its entire thickness rather than appearing only at the P3HT:PCBM interface. In contrast, little difference was observed in the oxide layers formed using target powers of 500 W or greater. The O/Al ratio remained constant, with layer thicknesses of 5–6 nm observed for each sample localized at the buried P3HT:PCBM interface; this is consistent with the presence of trace amounts of oxygen that react with the sputtered aluminum in proportion to the sputtering rate; this proceeds up to a limiting value where the oxygen becomes exhausted after producing a 5–6 nm thick oxide layer. The mechanism for creation of this buried oxide layer remains unclear, although many previous reports have speculated that chemical reactions are likely at such interfaces due to the highly energetic particle collisions inherent in the sputtering process.[12,14,16]

The Al/C ratio, indicative of the penetration of aluminum atoms into the organic films, follows a similar trend (with respect to sputtering target power) as that observed for the oxide formation (Figure 3b inset). There is an initial increase in the penetration depth with increasing sputtering power, with a penetration of approximately 3 nm observed at 100 W, increasing to 6–8 nm at 500 W. However, further increases in the target power up to a maximum of 1500 W did not create any further penetration of the aluminum atoms into the organic film. This penetration depth is identical to that typically observed for evaporated aluminum contacts using similar XPS measurements,[29] which indicates that the sputtering deposition technique does not generate excess penetration of aluminum into the organic layer as compared to standard physical vapor deposition techniques employed in high-efficiency small-scale devices. Furthermore, the penetration depth of the aluminum determined by the Al/C ratio is consistent with the penetration depth of the oxide layer determined from the O/Al ratio, which suggests that the majority of the penetrating aluminum is associated with the interfacial oxide layer. The data presented here therefore indicates that the major issue generated by sputtering metal contacts onto the organic films is not a penetration of energetic particles into the film, but rather the creation of a poorly conducting oxide barrier at the interface of the photoactive layer and the metal contact.

To confirm the findings of the XPS chemical analysis measurements, small-scale model devices were prepared with PEDOT:PSS hole-transport layers and a P3HT:PCBM pho-

 © 2015 Wiley-VCH Verlag GmbH & Co. KGaA, Weinheim

toactive layer. No electron transport layers were applied to highlight the influence of different sputtered cathode fabrication conditions on the device performance. Initially, thermally evaporated aluminum buffer layers of varying thickness were deposited prior to sputtering of the aluminum cathodes. This systematic creation of buffer layers using both a cathode material and deposition technique known to form relatively efficient charge extracting electrodes[30] allows the issue of sputtering penetration and film damage to be probed in greater detail. OPVs prepared by sputtering directly onto the active layer without any evaporated buffer showed extremely poor performance ($\eta < 0.02\,\%$) in both pristine and annealed devices. However, the addition of the evaporated aluminum buffer layers produced a significant improvement in device performance (Figure 4a). In particular, the addition of

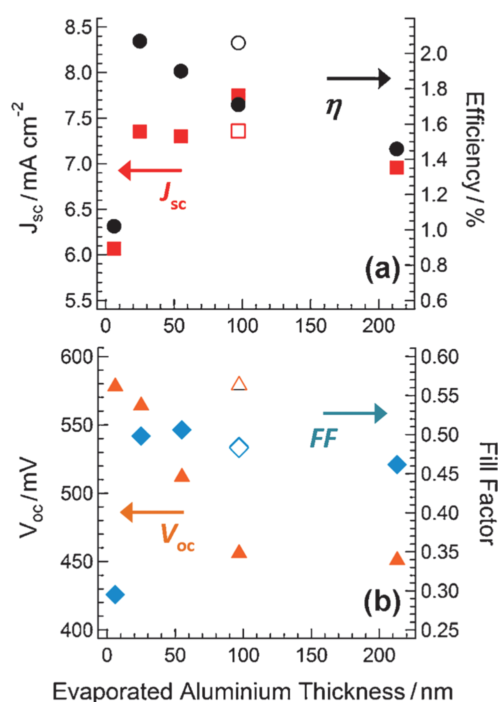

Figure 4. Photovoltaic performance data for annealed P3HT:PCBM devices fabricated with evaporated aluminum barriers of various thicknesses deposited prior to sputtering (solid symbols): a) V_{oc} (▲) and fill factor (◆), and b) J_{sc} (■), and device efficiency (●). The reference devices with no sputtering are shown as open symbols (△, ◇, □, ○) for each parameter.

a 6 nm buffer layer produced a device efficiency of 1.02 %, approximately half the value of the standard reference device with a fully evaporated cathode (2.06 %). The efficiency for devices with buffer layers of 25–55 nm were comparable to the evaporated-only standard, driven by a J_{sc} equal to, or slightly greater than that of the standard (7.36 mA cm^{-2}). For thicknesses greater than 55 nm, the device efficiency began to decrease, following a systematic decrease in the device V_{oc} with increasing evaporated aluminum buffer thickness (Figure 4b). As all samples possess identical hole-transporting and active layers, this result suggests a decreased charge density present in the aluminum cathode with increasing buffer layer thickness. Given that both the J_{sc} (Figure 4a) and fill factor (Figure 4b) of the devices are invariant and equal to the value of an evaporated-only reference device for samples with a buffer layer thickness greater than 25 nm, it is unlikely that the reduced charge density is related to charge generation or transport effects in the active layer. Instead, the V_{oc} drop appears likely to be caused by a cathode interface effect. We note that the sputtering process creates an oxide interface (Figure 3b), whereas the evaporated buffer produces a metallic interface with the active layer. The V_{oc} decrease appears to be correlated with an increase in the metallic character of the interface as the evaporated buffer layer thickness is increased. It is possible that the decreased V_{oc} is caused by a change in the cathode work function as aluminum oxide (3.8 eV) is systematically altered to pristine aluminum (4.3 eV);[31,32] however the exact mechanism remains unclear at this time.

The current density–voltage (J–V) curves of devices also support the presence of a space-charge-limited charge-extraction interface, exhibiting an S-shaped kink for pristine devices, which is subsequently transformed to a typical J-shaped diode curve upon annealing (Figure 5). The characteristics of

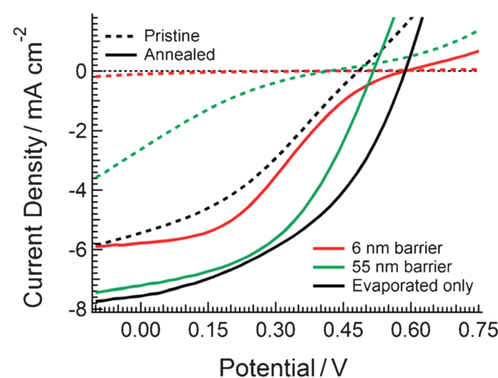

Figure 5. Current density voltage curves obtained under AM 1.5 illumination for P3HT:PCBM pristine (dashed lines) and annealed (solid lines) devices prepared with no sputtering (black), and with a 6 nm (red), and 55 nm (green) evaporated aluminum barrier deposited prior to sputtering.

the S-shaped curves are consistent with a charge-extraction barrier rather than an injection-limiting energetic barrier from a poorly matched electrode work function, in accordance with recently determined analytical parameters.[34] The S-shaped kink is not evident for the evaporated reference device, indicating that the charge-extraction barrier is created by the sputtering process. The pristine device prepared with a 55 nm evaporated barrier exhibits a small photoresponse ($\eta = 0.211\,\%$), with a significant S-shaped kink in the J–V curve, despite the sputtered material penetrating only 6–8 nm (11–15 %) into a deposited film as determined in the earlier XPS depth profiling. This result suggests that damage to the P3HT:PCBM film from penetration of sputtered ions can only be assigned a minimal role in the efficiency-limiting damage induced in an OPV using a sputtered cathode. The major source of the performance limitation is therefore de-

© 2015 Wiley-VCH Verlag GmbH & Co. KGaA, Weinheim

termined to be an aluminum oxide charge-extraction barrier created during the sputtering process.

The influence of the charge-extraction barrier was observed to be greatly diminished upon annealing the devices at 140 °C for 4 min, with a removal of the S-shaped kink in the *J*--*V* curves and an improvement in device performance by an order of magnitude. This observation is consistent with our previous research on degradation mechanisms in P3HT:PCBM devices, which found that degradation occurs following a combination of three primary pathways: (1) cathodic oxidation, (2) active layer phase segregation, and (3) anodic diffusion, some of which can be reversed upon thermal annealing.[35]

Given that the presence of an oxide charge-extraction barrier is the dominant reason for poor performance in sputtered devices, removing the conditions for its creation should provide a route towards viable sputtering of highly efficient devices on a R2R scale without the need for additional processing to cure the sputtering damage. The creation of an insulating oxide barrier during sputtering could potentially arise from two sources: (a) the presence of residual oxygen within the sample chamber during the sputtering process, (b) the impingement of pre-oxidized aluminum from the outer layer of the target exposed to air during venting of the chamber to remove the previous samples. All OPV devices prepared for this study had been previously sputtered after a single pump-purge cycle prior to sputtering, with a 5 s target activation period prior to sample deposition to remove the surface oxidized metal from the target. It was expected that with these conditions, the partial pressure of oxygen in the chamber (after evacuation to the level of 10^{-6} mTorr) would be negligible and the surface-oxidized material would be removed prior to deposition on the sample. However, it was noted that thermally evaporated cathodes are typically fabricated inside an inert atmosphere glove box, thus the pump–purge cycle for evaporated cathodes typically occurs from a much lower base partial pressure of oxygen. Furthermore, the sputter coater employed in this study has a much larger chamber due to its focus for large-area R2R deposition; therefore an equivalent partial pressure to that normally employed for sputtering will produce a larger amount of oxygen molecules in the larger chamber. To remedy this, additional efforts were employed to both remove oxygen sources from the sputtering chamber and to burn off the oxidized layer of the target prior to sputtering. A new sample was prepared after extensive pumping and purging of the chamber. The chamber was initially pumped to a base pressure of 10^{-7} mTorr, before back-filling with nitrogen to atmospheric pressure. This cycle was then repeated a further three times, noting that the time required to pump down the chamber reached a constant value on the last two pump-purge cycles. The target power was then applied and the plasma was allowed to remove the oxidized surface of the target for 30 s prior to moving the samples into the deposition zone. The *J*--*V* characteristics for the device prepared in this manner are compared to that of a thermally evaporated reference device in Figure 6 a.

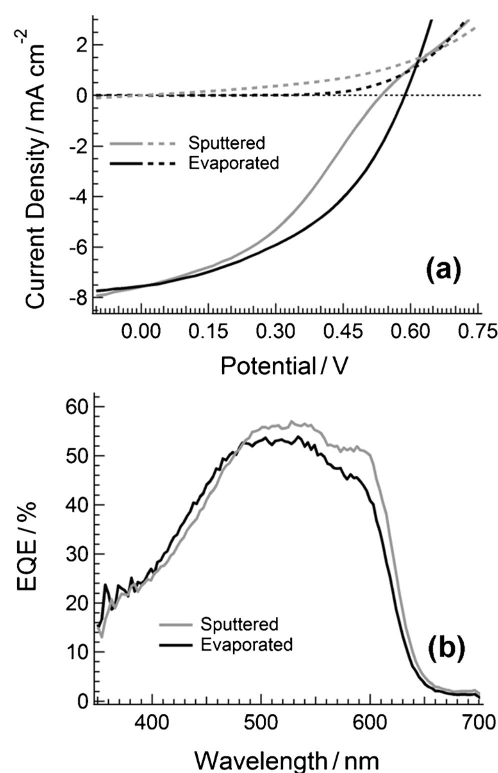

Figure 6. a) Current density–voltage curves obtained in the dark (dashed lines) and under AM 1.5 illumination (solid lines), and b) EQE curves for annealed P3HT:PCBM devices prepared with a sputtered (gray) or evaporated (black) aluminum cathode.

The photovoltaic device parameters for all fabricated devices are presented in Table 1. The sputtered device fabricated without any buffer layers in a reduced-oxygen environment shows comparable performance to the evaporated reference electrode. The J_{sc} of the devices is almost identical (7.57 mA cm^{-2} for sputtered and 7.34 mA cm^{-2} for evaporated), as confirmed by the closely matched external quantum efficiency (EQE) curves of both devices (Figure 6 b). The V_{oc} values of the sputtered and evaporated samples are also

Table 1. Photovoltaic performance parameters after annealing for P3HT:PCBM devices prepared using a range of different cathode fabrication conditions.

Cathode Fabrication Conditions	V_{oc} [mV]	J_{sc} [mA cm^{-2}]	*FF*	η [%]
evaporated Al only (100 nm)	579	7.36	0.483	2.06
evaporated Al (6 nm); then sputtered Al (100 nm)	578	6.07	0.295	1.02
evaporated Al (25 nm); then sputtered Al (100 nm)	564	7.36	0.498	2.07
evaporated Al (55 nm); then sputtered Al (100 nm)	512	7.30	0.506	1.90
evaporated Al (97 nm); then sputtered Al (100 nm)	456	7.75	0.485	1.71
evaporated Al (213 nm); then sputtered Al (100 nm)	451	6.96	0.462	1.46
sputtered Al Only (100 nm)	535	7.57	0.393	1.59

© 2015 Wiley-VCH Verlag GmbH & Co. KGaA, Weinheim

comparable, with values of 534 mV for the former and 579 mV for the latter. The major difference between the two samples is the lower fill factor for the sputtered device, resulting in a device efficiency reduction of 23 % from the evaporated reference value ($\eta = 2.06\,\%$) to the value for the sputtered sample ($\eta = 1.59\,\%$). Critically, the change in vacuum processing conditions clearly produces efficient OPV devices using sputtered cathodes without the need for any additional buffer layers. The slightly lower fill factor in the sputtered device with respect to the evaporated reference indicates that the vacuum processing procedure has not yet been optimized, and further efforts must be made to remove all residual oxygen sources from the sputtering chamber prior to cathode deposition. Furthermore, the devices prepared with the modified sputtering procedure compare quite favourably to the cell efficiencies of 1.5–2 % achieved for all-printed OPV devices that employ printed silver cathodes.[6] Further optimization of the vacuum processing procedure for sputter deposition and the introduction of suitable charge-selective buffer layers into the OPV structure offers great promise for further improving the performance of large-scale OPV modules fabricated using R2R printing and sputtering processes.

The results presented in this work highlight that sputtering of devices in a R2R environment is a feasible option to produce efficient operating devices. Furthermore, the addition of electron-transport layers to improve the efficiency will create a further barrier to protect the active layer and should allow for the fabrication of sputtered devices with comparable efficiencies to those of thermally evaporated cathodes.

Conclusions

This work has successfully demonstrated the fabrication of organic photovoltaic devices with aluminum cathodes sputtered onto P3HT:PCBM photoactive layers in a R2R process without creating significant efficiency losses or the need for further post-treatment. The optimal conditions for sputtering were found to be those that strike a compromise between uniform lateral coverage across the PET roll, reduced power for minimizing the energetic particle damage to organic films, and fast aluminum deposition rates. X-ray photoelectron spectroscopy (XPS) analysis of films sputtered using various powers found that a 5–6 nm insulating oxide layer was generated at the interface between the active layer and the cathode for all sputtering target powers greater than 500 W. Further analysis of the aluminum penetration into the P3HT:PCBM film showed a constant penetration depth of 6–8 nm, consistent with the thickness of the oxide layer and suggesting that aluminum penetration into the organic film is not the major reason for performance limitations in sputtered devices. Introduction of thermally evaporated aluminum buffer layers of varying thickness prior to deposition of sputtered aluminum cathodes found that the performance of devices after annealing matched those of reference devices prepared with no sputtering for a buffer thickness of only 20 nm. Further analysis of the device *J*--*V* curves found that the major reason for the poor performance in devices was the presence of a charge-extraction barrier at the cathode, which was removed upon subsequent annealing of devices. The S-shaped kink remained present in samples with thick evaporated aluminum buffer layers, suggesting that the creation of an oxide layer during sputtering was the dominant reason for poor performance in the sputtered devices rather than penetration of ions into the organic film. Careful removal of oxygen from the sputtering chamber prior to aluminum deposition onto the P3HT:PCBM active layer was subsequently observed to produce a device with an efficiency close to that of the thermally evaporated reference device without any additional buffer layers required. The exciting results presented in this work highlight that sputtering of devices in a roll-to-roll environment is a feasible option to produce highly efficient operating devices.

Experimental Section

OPV Film Fabrication

Pre-patterned ITO-coated glass substrates (Xinyan Technologies, $R_{sheet} < 15\ \Omega/\square$) were cleaned by successive sonication in detergent, deionized water, and isopropanol for 10 min each. Cleaned electrodes were then exposed to a UV-ozone treatment for 15 min. A PEDOT:PSSS hole-transporting layer (Heraeus, HTM solar) was deposited onto a glass substrate layer by spin coating at 4000 rpm for 60 s, then drying at 140 °C for 30 min to produce a film thickness of 35 nm. Active layer blend solutions were prepared in chloroform using P3HT (fabricated in-house with a molecular weight of 44 kDa) and PCBM (Solenne) in a ratio of 1:0.8 wt % (P3HT/PCBM) with a total blend concentration of 20 mg mL^{-1}. Active layers were deposited onto the PEDOT:PSS by spin coating at 800 rpm for 60 s. Samples were subsequently cured at 60 °C for 5 min and then transferred to a glove box prior to cathode deposition.

Thermal Evaporation of Aluminum Cathodes

Device films were secured inside a mask, placed into a multi-source thermal evaporator, and evacuated down to a pressure of 10^{-6} mTorr. A 100 nm aluminum cathode was then evaporated at 0.2 nm s^{-1} onto the active layer through the shadow mask, which defined the active area of the cells to be 14 mm^2. After fabrication, the OPV devices were transferred to a glove box where they were annealed at 160 °C for 5 min before performance evaluation. Devices were transferred between the thermal evaporator and R2R sputter coater inside a sealed container filled with nitrogen.

Roll-to-Roll Sputter Coating of Aluminum Cathodes

Sputter coating of aluminum cathodes was performed using custom-built R2R equipment purchased from Semicore Equipment, Inc. The system is comprised of two terminal 7 cm spindles, which maintained the tension across a 300 mm PET web through winding and rewinding processes (controlled by customized Pro487 software from Semicore). The web is driven through a series of rollers using Allen–Bradley control motors before travelling around a water-cooled 22.9 cm drum where it is exposed to 3 consecutive deposition zones from individually con-

© 2015 Wiley-VCH Verlag GmbH & Co. KGaA, Weinheim

trolled targets. The sputtering chamber is evacuated to low vacuum (0.1 mTorr) with a Trivac D40B-D65B roughing pump (Oerlikon Leybold Vacuum) and then further evacuated to a high vacuum base pressure (10^{-6} mTorr) using a water-chilled Cryo-Torr pump (Helix Technologies). Sputtering was performed in an argon plasma created using a direct current (DC) magnetron; with power supplied to the 35.6×10.1 cm^2 aluminum targets (Angstrom Sciences, Inc.) using separate 6 kW Pinnacle DC power sources (Advanced Energy Industries, Inc.)

Initial optimization studies employed a range of different sputtering pressures and target powers to examine the aluminum deposition behaviour on PET substrates. Sputtered cathodes for all OPV films in this study were subsequently prepared using a deposition time of 42 s at a sputtering base pressure of 5×10^{-6} mTorr, a process pressure of 2 mTorr, and a target power of 1.5 kW (power density = 4.15 W cm^{-2}). OPV films were secured to the rotating drum inside the coating chamber and sputtered through a shadow mask applied to the samples with Kapton tape.

J--V and EQE Testing

Current density–voltage (*J–V*) measurements were performed using a Newport Class A solar simulator with an AM 1.5 spectrum filter. The light intensity was calibrated to 100 mW cm^{-2} using a silicon reference solar cell (FHG-ISE). *J--V* data were recorded in the dark and under illumination uing a Keithley 2400 source meter. Individual devices were masked to an illuminated area of 3.8 mm^2 to eliminate additional photocurrent responses from neighboring devices on the common substrate. External quantum efficiency measurements were recorded by illuminating the devices with a tungsten halogen lamp passed through an Oriel Cornerstone 130 monochromator. An Ithaco Dynatrac 395 analogue lock-in amplifier and Thorlabs PDA55 silicon diode were employed to collect the reference signal, and a Stanford Research Systems SR830 DSP digitizing lock-in amplifier was employed to measure the device current.

UV-Visible Spectrophotometry

The optical densities of the PET substrates coated with aluminum films using various sputtering parameters were determined using a Varian Cary 6000i UV-vis spectrophotometer equipped with sample transport and thin film holder accessories. As the transport stage provides a maximum translation of 160 mm, the 300 mm web was cut in half prior to mounting in the sample holder. The lateral zero position was calibrated to be adjacent to the outer edge of the web, whereas the center of the sputtered web occurred at a sample translation of 150 mm. Due to the high optical density of the sputtered films, absorbance measurements were performed using the rear-beam attenuator accessory set to an attenuation of optical density (OD) 1.7 to reduce the dynamic range required for the highly absorbing samples. Absorbance spectra were measured with reference to an uncoated PET substrate over the range 400–1000 nm, with spectra acquired in 25 mm steps from the zero position towards the centre of the web. The thicknesses of films were determined from the average of 9 individual absorbance values at wavelengths between 700 nm and 900 nm (in 25 nm steps) using published aluminum attenuation coefficients.[36]

X-ray Photoelectron Spectroscopy Measurements

Depth profiles were acquired using X-ray photoelectron spectroscopy and an argon gas cluster ion source for sample etching. Argon clusters of a mean size 500 atoms were accelerated to 20 keV for a mean energy per atom of 40 eV. After each 15-second etch cycle, a survey XPS spectrum was acquired using monochromated Al K-alpha radiation and a pass energy of 160 eV.

Acknowledgements

This research was primarily funded by the Australian Research Council through its Discovery Grant Scheme (Project DP140104083). The authors acknowledge the use of equipment as well as scientific and technical assistance of the WA X-Ray Surface Analysis Facility, funded by the Australian Research Council LIEF Grant Scheme (Project LE120100026). The work was also performed in part at the Materials node of the Australian National Fabrication Facility, a company established under the National Collaborative Research Infrastructure Strategy to provide nano- and microfabrication facilities for Australia's researchers.

Keywords: aluminum · photovoltaics · printing · roll-to-roll processing · sputter coating

[1] G. Dennler, M. C. Scharber, C. J. Brabec, *Adv. Mater.* **2009**, *21*, 1323.
[2] R. R. Søndergaard, M. Hösel, F. C. Krebs, *J. Polym. Sci. B* **2013**, *51*, 16.
[3] C. J. Mulligan, M. Wilson, G. Bryant, B. Vaughan, X. Zhou, W. J. Belcher, P. C. Dastoor, *Solar Energy Mater. Solar Cells* **2014**, *120*, 9.
[4] J. Adams, G. D. Spyropoulos, M. Salvador, N. Li, S. Strohm, L. Lucera, S. Langner, F. Machui, H. Zhang, T. Ameri, M. M. Voigt, F. C. Krebs, C. J. Brabec, *Energy Environ. Sci.* **2015**, *8*, 169.
[5] M. Hösel, R. R. Søndergaard, M. Jørgensen, F. C. Krebs, *Energy Technol.* **2013**, *1*, 102.
[6] a) M. Pagliaro, R. Ciriminna, G. Palmisano, *Prog. Photovolt. Res. Appl.* **2010**, *18*, 61; b) F. Krebs, N. Espinosa, M. Hösel, R. R. Søndergaard, *Adv. Mater.* **2014**, *26*, 29; c) P. Sommer-Larsen, M. Jørgensen, R. R. Søndergaard, M. Hösel, F. C. Krebs, M. Jørgensen, *Energy Technol.* **2013**, *1*, 15.
[7] F. C. Krebs, R. Søndergaard, M. Jørgensen, *Solar Energy Mater. Solar Cells* **2011**, *95*, 1348.
[8] H. Fujimoto, W. J. Potscavage, Jr., T. Edura, C. Adachi, *Org. Electron.* **2014**, *15*, 2783.
[9] S. B. Sapkota, M. Fischer, B. Zimmermann, U. Würfel, *Solar Energy Mater. Solar Cells* **2014**, *121*, 43.
[10] K. Sivakumar, S. M. Rossnagel, *J. Vac. Sci. Technol. A* **2010**, *28*, 515.
[11] J. Perelaer, P. J. Smith, D. Mager, D. Soltman, S. K. Volkman, V. Subramanian, J. G. Korvink, U. S. Schubert, *J. Mater. Chem.* **2010**, *20*, 8446.
[12] A. Iwan, M. Palewicz, M. Ozimek, A. Chuchmala, G. Pasciak, *Org. Electron.* **2012**, *13*, 2525.
[13] L. S. Liao, L. S. Hung, W. C. Chan, X. M. Ding, T. K. Sham, I. Bello, C. S. Lee, S. T. Lee, *Appl. Phys. Lett.* **1999**, *75*, 1619.
[14] S. M. Rossnagel, *J. Vac. Sci. Technol. A* **1989**, *7*, 1025.
[15] C. J. Traverse, M. Young, S. Wagner, P. Zhang, P. Askeland, M. C. Barr, R. R. Lunt, *J. Appl. Phys.* **2014**, *115*, 194505.
[16] Y. Jouane, S. Colis, G. Schmerber, C. Leuvrey, A. Dinia, P. Lévêque, T. Heisera, Y.-A. Chapuis, *J. Mater. Chem.* **2012**, *22*, 1606.
[17] L. S. Hung, L. S. Liao, C. S. Lee, S. T. Lee, *J. Appl. Phys.* **1999**, *86*, 4607.

© 2015 Wiley-VCH Verlag GmbH & Co. KGaA, Weinheim

[18] T. H. Gil, C. May, S. Scholz, S. Franke, M. Toerker, H. Lakner, K. Leo, S. Keller, *Org. Electron.* **2010**, *11*, 322.
[19] H. Fujimoto, T. Miyayama, N. Sanada, C. Adachi, *Org. Electron.* **2013**, *14*, 2994.
[20] J. Hanisch, E. Ahlswede, M. Powalla, *Thin Solid Films* **2008**, *516*, 7241.
[21] E. Ahlswede, J. Hanisch, M. Powalla, *Appl. Phys. Lett.* **2007**, *90*, 063513.
[22] J. Hanisch, E. Ahlswede, M. Powalla, *Eur. Phys. J. Appl. Phys.* **2007**, *37*, 261.
[23] T. H. Gil, C. May, H. Lakner, K. Leo, S. Keller, *Plasma Process. Polym.* **2009**, *6*, S808.
[24] H. Suzuki, M. Hikita, *Appl. Phys. Lett.* **1996**, *68*, 2276.
[25] B. Arredondo, C. de Dios, R. Vergaz, A. R. Criado, B. Romero, B. Zimmermann, U. Würfel, *Org. Electron.* **2013**, *14*, 2484.
[26] D. Kaduwal, H.-F. Schleiermacher, J. Schulz-Gericke, T. Kroyer, B. Zimmermann, U. Würfel, *Solar Energy Mater. Solar Cells* **2014**, *124*, 92.
[27] P. Kubis, L. Lucera, F. Machui, G. Spyropoulos, J. Cordero, A. Frey, J. Kaschta, M. M. Voigt, G. J. Matt, E. Zeira, C. J. Brabec, *Org. Electron.* **2014**, *15*, 2256.
[28] A. G. Shard, R. Havelund, M. P. Seah, S. J. Spencer, I. S. Gilmore, N. Winograd, D. Mao, T. Miyayama, E. Niehuis, D. Rading, R. Moellers, *Anal. Chem.* **2012**, *84*, 7865.
[29] K. Feron, C. J. Fell, L. J. Rozanski, B. B. Gong, N. Nicolaidis, W. J. Belcher, X. Zhou, E. Sesa, B. V. King, P. C. Dastoor, *Appl. Phys. Lett.* **2012**, *101*, 193306.
[30] Y. S. Eo, H. W. Rhee, B. D. Chin, J.-W. Yu, *Synth. Met.* **2009**, *159*, 1910.
[31] V. K. Agarwala, T. Fort, Jr., *Surf. Sci.* **1976**, *54*, 60.
[32] Y. Vaynzof, T. J. Dennes, J. Schwartz, A. Khan, *Appl. Phys. Lett.* **2008**, *93*, 103305.
[33] W. Tress, O. Inganäs, *Solar Energy Mater. Solar Cells* **2013**, *117*, 599.
[34] P. Kumar, C. Bilen, K. Feron, X. Zhou, W. J. Belcher, P. C. Dastoor, *Appl. Phys. Lett.* **2014**, *104*, 193905.
[35] P. Kumar, C. Bilen, K. Feron, N. C. Nicolaidis, B. B. Gong, X. Zhou, W. J. Belcher, P. C. Dastoor, *ACS Appl. Mater. Interfaces* **2014**, *6*, 5281.
[36] M. N. Polyanskiy, *Refractive Index Database*, http://refractiveindex.info, accessed April 18 **2014**.

Received: November 9, 2014
Revised: December 24, 2014
Published online on February 12, 2015

© 2015 Wiley-VCH Verlag GmbH & Co. KGaA, Weinheim